Towards Transparent Geohazard Model: XAI for Ground Deformation Susceptibility in Rhenish Coalfields, Germany

Dibakar Kamalini Ritushree [1,2], Marzieh Baes [2], Mahdi Motagh [1,2]

[1] GFZ Helmholtz Center for Geosciences, Potsdam, Germany – dibakar, marzieh.baes, mahdi.motagh @gfz.de

[2] Institute of Photogrammetry and GeoInformation, Leibniz University Hannover, Germany

Keywords: Coal Mining, Ground Deformation, Susceptibility Mapping, Machine Learning, eXplainableAI.

Abstract

Land subsidence is a significant geohazard in the Rhineland coalfields of Germany, primarily driven by large-scale open-pit mining and associated groundwater changes. This study integrates geospatial, geological, hydrological, and remote sensing datasets, including European Ground Motion Service (EGMS) measurements, to model subsidence susceptibility using a LightGBM classifier. The model demonstrates strong predictive performance in classifying four susceptibility levels (Low, Moderate, High and Very High). To enhance interpretability, Explainable Artificial Intelligence (XAI) techniques including PFI, LIME and SHAP were employed to identify key drivers of subsidence. Results consistently indicate that distance from mines and groundwater level are the dominant controlling factors, while faults and lithology provide secondary structural influence. Terrain and land cover variables contribute minimally. The integration of XAI proves critical in understanding model behavior, enabling not only accurate prediction but also transparent identification of underlying physical drivers. This improves confidence in the results and supports their application in risk assessment and mitigation planning. Field observations further validate that high-susceptibility zones correspond to areas of observed structural damage, confirming the reliability of the proposed framework.

1. Introduction

1.1 Motivation

The rapid growth of Earth observation data has made satellite remote sensing an indispensable tool for disaster monitoring and environmental management, offering consistent, large-scale observations of Earth’s surface dynamics. Leveraging these extensive datasets, machine learning (ML) has emerged as a powerful means to extract complex patterns and predict geohazards. Among these hazards, ground deformation induced by coal mining poses severe risks to infrastructure, ecosystems, and nearby communities(Bai et al., 2025; Firozjaei et al., 2021; Lian et al., 2021; Tang et al., 2020). Timely identification of deformation-susceptible zones is therefore critical for effective risk mitigation and resilience planning. Recent research highlights the growing importance of data-driven approaches for evaluating subsidence hazards in diverse geological environments (Liu et al., 2024; Qiu et al., 2023; Rahmati et al., 2019). Advanced computational models have been applied to uncover the underlying causes of ground deformation, assess fissure susceptibility in fragile zones(Al-Masnay et al., 2022), and support early warning frameworks using satellite-based time-series observations (Mirmazloumi et al., 2023). The integration of satellite interferometry with intelligent algorithms enables near real-time monitoring of surface deformation, significantly improving hazard preparedness (Zhou et al., 2024). These approaches are capable of capturing nonlinear interactions among environmental and anthropogenic variables that are often overlooked by conventional techniques (Adadi and Berrada, 2018). As a result, they provide a more reliable basis for identifying high-risk zones and understanding subsurface processes. To address this need, this study develops an interpretable machine learning framework that integrates multi-source geospatial data with eXplainable Artificial Intelligence (XAI) techniques to map ground deformation susceptibility across the Rhineland open-pit coal mining areas, which are currently operational. Unlike traditional black-box models, the proposed approach provides insight into the driving factors such proximity to mines and faults, groundwater change, and topographical aspects, enabling stakeholders to plan land use more safely, restrict development in high-risk zones, and strengthen continuous monitoring for disaster risk reduction.

1.2 Study Area

The study focuses on the Rhenish coalfield in North Rhine-Westphalia, Germany, one of Europe’s largest lignite mining regions, encompassing the Hambach, Garzweiler, and Inden open-pit mines operated by RWE Power AG, as shown in Figure1.

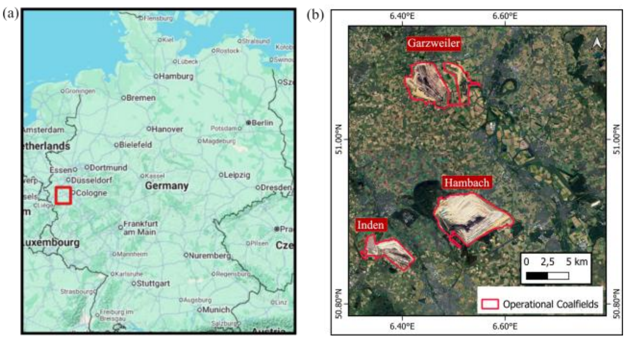

Figure 1. (a) The location of the Rhineland Coalfields in Germany, (b) Currently operational mines. (c) (d), (e) and (f) are field evidence of damage as a consequence of the open pit mining in these regions.

Continuous mining for over a century has reshaped the landscape, causing significant ground deformation (Ritushree et al., 2026; Tang et al., 2020) and requiring large-scale village relocations. Current mining areas cover approximately 9,700 ha, with an annual production capacity of up to 120 Mt of lignite. The

https://doi.org/10.5194/isprs-archives-XLIX-B2-2026-737-2026

ongoing subsidence could be clearly visualized in Figure 2, where the European Ground Motion Service (EGMS) Ortho product showcases the ground motion from 2019-2022. The ground motion in the study area over a five-year period reaches subsidence rates of up to approximately 11 cm/yr, predominantly localized around the active mining regions.

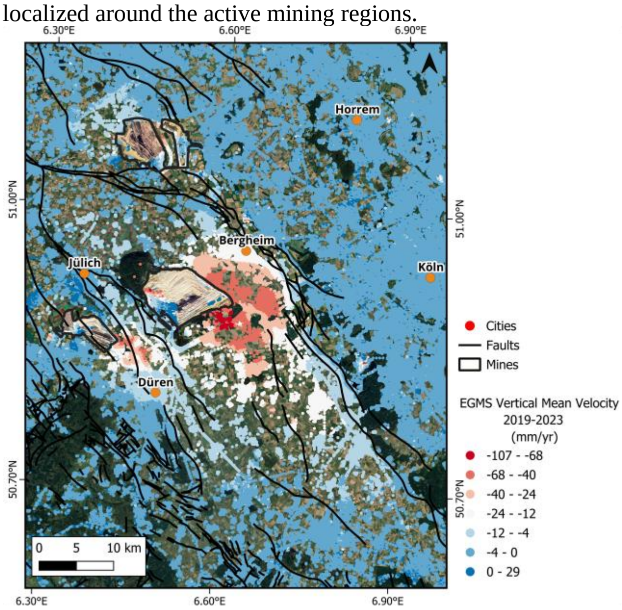

Figure 2. European Ground Motion Service (EGMS) vertical mean velocity map showing subsidence patterns (in black) along the periphery of the coalfields, with major fault structures also indicated (black), highlighting their spatial association with ground deformation.

2. Data and Methodology

2.1 Remote Sensing Data

The study integrates multi-source geospatial datasets to capture factors influencing ground deformation. Geological data, including lithology and structural features, were obtained from the GUEK250 map(BGR (2016), n.d.)with major faults mapped as key boundaries. Groundwater information for the shallow aquifer from 1955–2022 provided mean annual levels and cumulative fluctuations provided by Erftverband Company. Topographic parameters i.e, slope, aspect, and curvature were derived from the Copernicus 10 m DEM. Vegetation cover was represented by NDVI computed from Sentinel-2 imagery, also resampled to 30 m. Proximity layers, including distances to faults, rivers, and mining areas, captured the spatial influence of both natural and anthropogenic stressors. These datasets (Figure. 3) together formed the feature set for the machine learning model, used to predict ground deformation susceptibility. The workflow for the methodology used in this study is illustrated in Figure 4. In this study, the reference data were derived from the EGMS Level 3 Ortho product(Crosetto et al., 2026). Mean vertical velocity values were categorized into four susceptibility classes: > –4 mm/year (Low), –4 to –7 mm/year (Moderate), –7 to –13 mm/year (High), and < –13 mm/year (Very High). These thresholds were not arbitrarily selected but informed by established European engineering and geotechnical frameworks (The Council for the Environment and Infrastructure, 2020) and validated against the statistical distribution of the EGMS dataset. It is further supported by empirical observations (Wolersdorfer and Thiem, 1999) of subsidence in sandy soils under open-pit mining to ensure their geological relevance and consistency with observed deformation patterns.

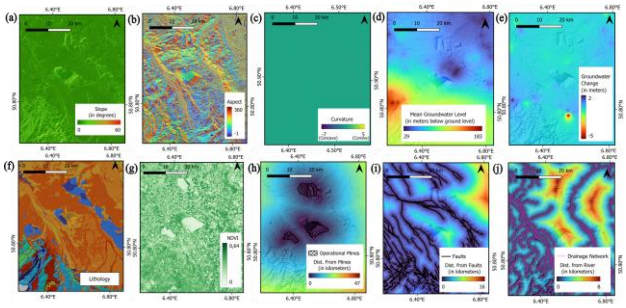

Figure 3. Feature set used for the training, in the study: (a)Slope (b)Aspect (c)Curvature (d)Mean Groundwater Level(GWL) (e) Groundwater Change(GWL_Change) (f) Lithology (g) NDVI (h) Distance from Mines(Dist_Mines)) (i) Distance from Faults(Dist_Faults) and (j) Distance from rivers(Dist_River).

2.2 Pre-processing of Input Features

For training the model the features obtained from multiple sources in varying formats and coordinate systems, were standardized by georeferencing to a common coordinate reference system (EPSG:32632) and harmonizing resolution to 30 meters in ArcGIS. Multicollinearity among the variables was assessed using Pearson correlation coefficient shown in Figure 5. A threshold of Pearson’s r > 0.5 was used to indicate significant multicollinearity.

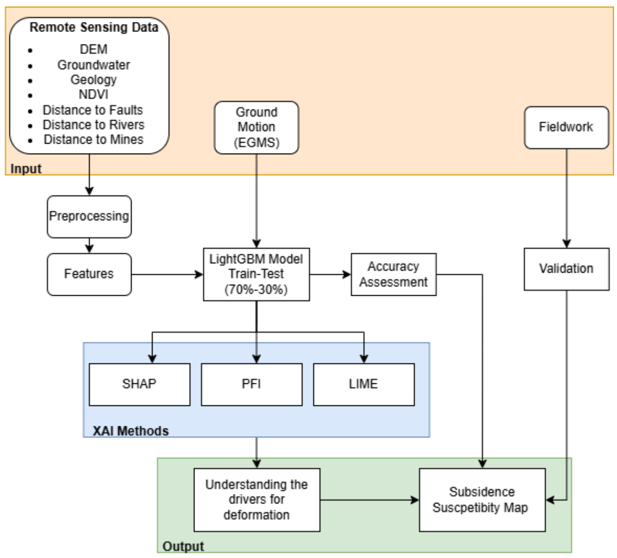

Figure 4. Workflow of the methodology showcasing the input provided, ML processing and final

The results showed that none of the variables exceeded these thresholds, confirming low interdependence among features. Consequently, all eight conditioning factors were retained for model training in the ground subsidence susceptibility assessment.

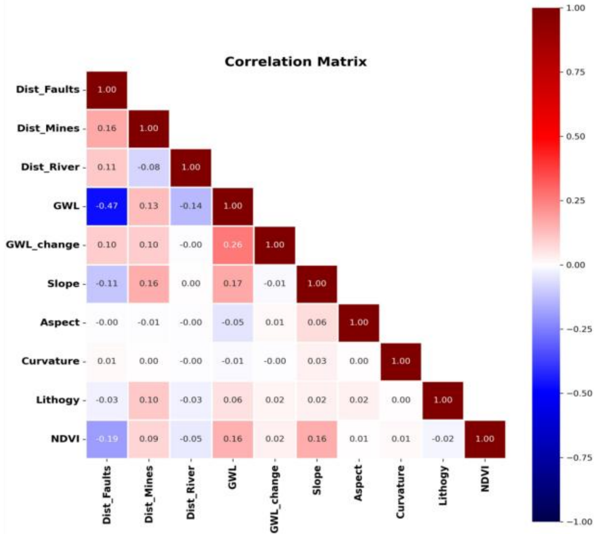

Figure 5. Multicollinearity analysis for features.

2.3 Machine Learning Model

LightGBM(Ke et al., 2017) is used for training and testing for hazard classification for our study. This model is chosen for the gradient boosting framework designed for high efficiency, low memory usage, and scalability, particularly suitable for complex datasets. It employs a leaf-wise tree growth strategy, where the leaf with the highest loss reduction is selected for splitting. During training, LightGBM iteratively builds decision trees by minimizing residual errors through gradient and Hessian information. In multi-class settings, separate trees are constructed for each class to optimize the overall objective function.

To ensure robust model evaluation and reduce potential overfitting, a minimal set of hyperparameters was adopted for the LightGBM multi-class model, including a learning rate of 0.1, 100 estimators, num_leaves of 31, and default regularization and subsampling parameters, ensuring a balance between model performance and generalization without extensive tuning. Also cross-validation was applied during training, providing a more reliable estimate of model generalization performance.

2.4 XAI Methods

We used the following XAI methods for the interpreting the classifer prediction for understanding the complex relationship triggering the subsidence in the study area.

SHAP (SHapley Additive exPlanations) quantifies the contribution of each feature to a prediction based on game-theoretic principles, providing consistent and theoretically grounded attributions for every prediction (Lundberg & Lee, 2017).

LIME (Local Interpretable Model-agnostic Explanations) approximates the model locally with a simple interpretable model to explain individual predictions, focusing on local rather than global behavior (Ribeiro et al., 2016).

PFI (Permutation Feature Importance) measures the decrease in model performance when a feature's values are randomly shuffled, giving a global view of feature relevance (Breiman, 2001).

Table 1 summarizes the trade-offs among the feature-interpretation methods used. It highlights differences in scope (global vs. local), computational cost, and explanation granularity.

XAI Methods	Trade-offs
PFI	Doesn't specify how the feature influences the outcome (positive vs. negative).
LIME global	Doesn't explain why any single location got its score, only what happens on average.
SHAP Summary	Simplicity and Computational speed/cost

Table 1. Tradeoffs among each XAI Methods

Together, these methods provide a comprehensive understanding: permutation importance identifies which features matter most overall, SHAP shows precise contributions per prediction, and LIME explains model behavior in specific local regions, allowing for robust insights into both global and local model behavior.

3. Results and Discussion

3.1 Model performance and Accuracy Assessment

The LightGBM model demonstrated strong performance on the test set, achieving an overall accuracy of 0.940 and a mean Intersection-over-Union (IoU) of 0.75. Class-specific performance was highest for the Low subsidence class (F1-score = 0.97, IoU = 0.94) and remained strong for the Very High class (F1-score = 0.89, IoU = 0.80). Moderate and High subsidence classes exhibited slightly lower performance (F1-scores ≈ 0.77 and 0.77, IoUs ≈ 0.62 and 0.62, respectively), reflecting the inherent difficulty of distinguishing intermediate subsidence rates. Overall, the results indicate that the model reliably captures both extreme and moderate subsidence patterns while maintaining realistic confidence across classes.

The precision–recall curve shown in Figure 6, further highlights the model's discriminative capability across subsidence classes. The area under the PR curve is highest for the Low class (1.00), indicating near-perfect separability, followed by Very High (0.97), High (0.92), and Moderate (0.91) classes. These results suggest that the model is highly effective at distinguishing both extreme and stable conditions, while maintaining strong performance for intermediate classes.

Predictive uncertainty in the LGBM model is highest along transition zones between subsidence classes, as indicated by the bright areas in the entropy maps. Entropy values range from 0 (dark, confident predictions) to 0.32 (bright, uncertain predictions), highlighting areas where subsidence rates vary gradually and making these regions naturally harder to classify. These zones correspond to regions where the faults are present and also shown in Figure7(b) gradually, rather than abruptly, leading to inherently ambiguous ground-truth labels. Since the model must assign a single discrete class to each pixel, it is less confident where conditions fall between defined classes, resulting in higher entropy. The concentration of uncertainty along these boundaries, particularly for High and Very High subsidence classes, reflects the model's realistic behavior, it expresses low confidence precisely where the data themselves are ambiguous, rather than distributing uncertainty randomly. Such patterns highlight areas where subsidence rates are gradually varying, making them naturally harder to classify.

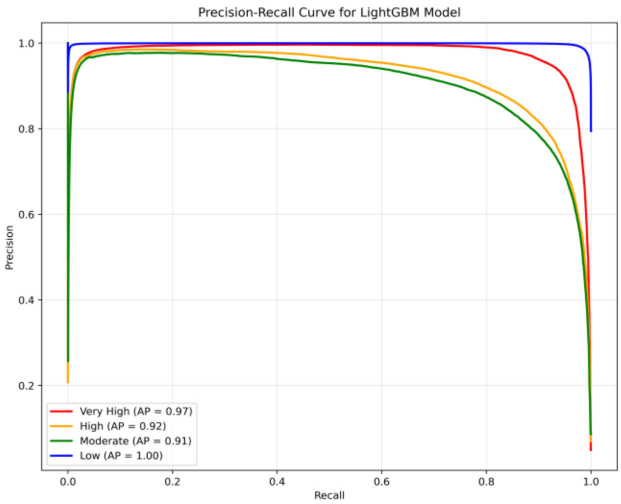

Figure 6. Precision–recall (PR) curves for the LightGBM model across subsidence hazard classes (Low, Moderate, High, and Very High), demonstrating strong class-wise discriminative performance, with highest separability observed for the Low and Very High classes.

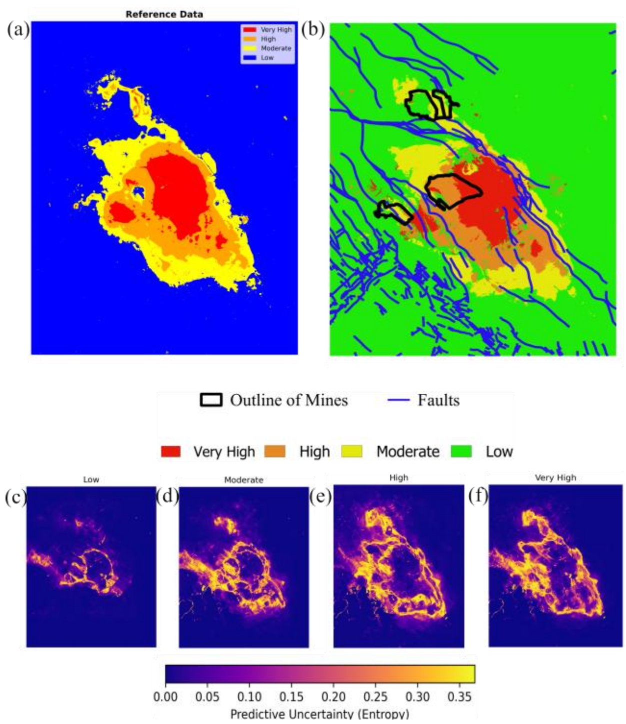

Figure 7. Subsidence susceptibility classification results produced by the model: (a) reference ground truth map showing four classes (Low, Moderate, High, and Very High); (b) LightGBM prediction with mapped faults and mining areas overlaid for spatial context. The lower panels present class-wise predictive uncertainty (entropy), highlighting areas of lower confidence, particularly along transition zones between classes: (c) Low, (d) Moderate, (e) High, and (f) Very High susceptibility.

While predictive uncertainty maps provide insight into the model's confidence, they do not directly measure how accurate the predictions are with respect to the reference data. Therefore, pixel differencing was performed as a complementary evaluation to quantify the actual agreement between predicted and ground truth classes illustrated in Figure 8.

The uncertainty (entropy) highlights where the model is less confident typically along transition zones but it does not indicate whether predictions in those areas are correct or incorrect. In contrast, pixel-wise differencing explicitly measures classification error by comparing predicted and true labels at each location. Together, these approaches provide a more comprehensive assessment.

To evaluate pixel-wise agreement between the predicted and reference maps, Mean Absolute Error (MAE) and Root Mean Square Error (RMSE) were employed as quantitative accuracy metrics. The low error values obtained from pixel differencing (MAE = 0.05 and RMSE = 0.25) indicate a high level of agreement between the predicted and reference subsidence classes. The very small MAE suggests that, on average, the predicted class labels deviate only minimally from the ground truth, implying that most pixels are either correctly classified or differ by only one adjacent class. Similarly, the relatively low RMSE indicates that larger misclassifications are infrequent and limited in magnitude. Together, these metrics confirm that the classification performance is robust and reliable, with errors primarily confined to transition zones between classes rather than widespread misclassification across the study area.

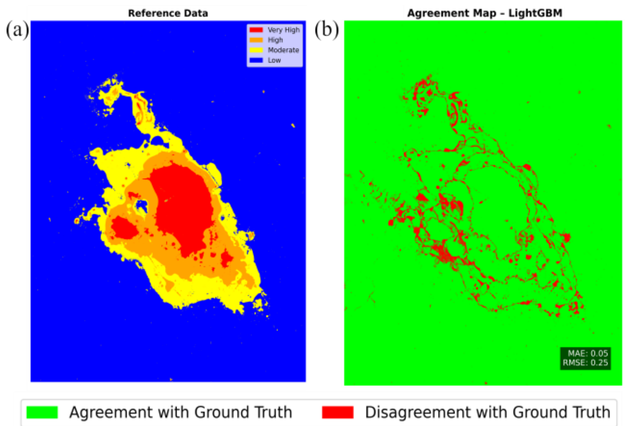

Figure 8. Pixel differencing based on the (a) Reference data (Ground truth in this study) and (b) the LightGBM classified hazard map.

3.2 XAI Analysis

PFI results in Figure 9 shows how much each geospatial predictor affects your LGBM subsidence model's accuracy when randomly shuffled. It highlights that mining activity is by far the strongest driver of subsidence in the study area, with proximity to mines achieving the highest importance value (~0.21). Mean Groundwater level and Groundwater fluctuations follow as the following most influential factor (~0.17 and ~0.15), reflecting the physically sensible role of hydrogeology in subsidence. Distance from faults (~0.07) and lithology (~0.06) indicate moderate influence. They capture the effects of structural geology and soil/rock compaction potential. Distance from rivers, topographic features such as slope, aspect and NDVI show low importance (<0.05), which is consistent with their minimal direct contribution. They retained to capture local effects, prevent omitted variable bias, and maintain interpretability.

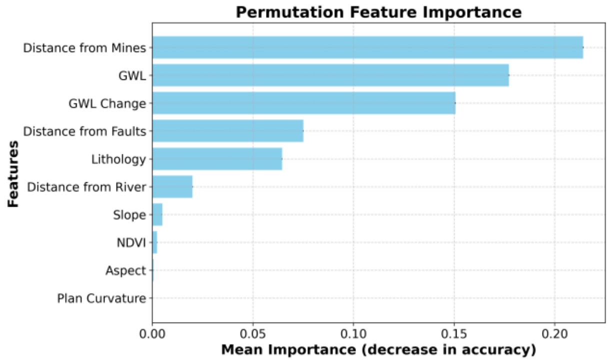

Figure 9. PFI results conducted on the test set of LightGBM model.

The curvature feature in this study area is largely homogeneous, exhibiting little spatial variation. As a result, it contributes minimally to the classification and receives a near-zero importance value. This outcome demonstrates that the feature attribution method effectively identifies variables that are truly relevant for the model, reflecting the model’s ability to prioritize physically meaningful predictors while ignoring features that provide no additional information. Overall, the rankings confirm that the model correctly prioritizes primary physical drivers while accounting for hydrogeological and structural controls, with minor features providing supporting context for localized influences.

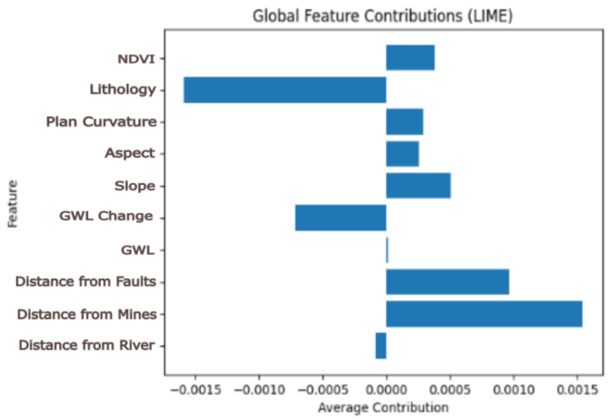

Figure10. LIME results conducted on the test set of LightGBM model.

Although LIME is primarily designed to explain individual, localized predictions, we aggregated the local explanations across all pixels to derive an average contribution for each feature, effectively providing a global perspective on feature importance for subsidence susceptibility. In this approach, features with positive average contributions increase the likelihood of higher subsidence, while features with negative contributions decrease it. LIME results highlights the key drivers of subsidence susceptibility in the model. Distance from mines is the strongest positive contributor (~0.0015), indicating that proximity to mining areas greatly increases the likelihood of higher subsidence. Lithology is the most significant negative driver (~ -0.0016), showing that certain rock types inhibit subsidence. Secondary positive contributors include distance from faults (~0.0010), slope (~0.0005), and NDVI (~0.0004), reflecting the roles of structural geology, terrain steepness, and vegetation density. Some features act as inhibitors**:** groundwater level (GWL) change (~ -0.0007) reduces the predicted probability of high subsidence, and distance from rivers (~ -0.0001) has a minor negative influence. These values demonstrate how both anthropogenic and natural factors combine to drive subsidence patterns in the study area.

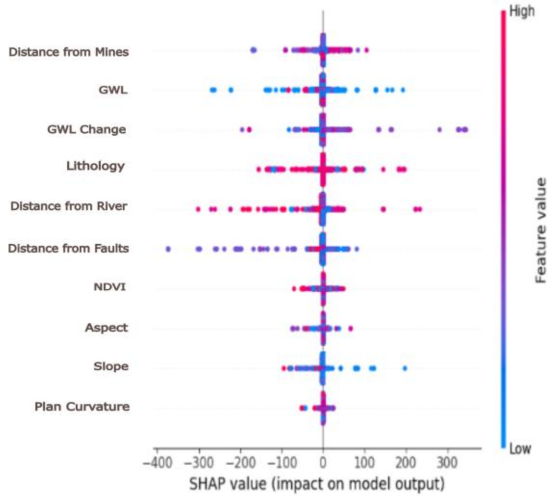

Figure 11. SHAP results conducted on the test set of LightGBM model.

In the SHAP summary plot shown in Figure 11, the Y-axis lists features ranked by overall importance, with the most influential feature at the top. The X-axis shows SHAP values, representing each feature’s impact on the model’s output: points to the right increase the predicted probability of subsidence, while points to the left decrease it. The color scale reflects the actual feature values, with red indicating high values and blue indicating low values. The vertical density of points indicates how many data instances fall within that SHAP value range, highlighting the distribution of feature effects across the dataset.

The SHAP summary plot ranks features by their mean absolute Shapley values, reflecting each feature’s overall influence on the model’s predictions. In the context of this study, the ranking distinguishes primary triggers for subsidence in the region**.** Distance from mines, the top-ranked feature, serves as the model’s primary geographical anchor: higher distances (red points) push predictions toward stability, indicating that the model first evaluates whether an area falls within a mining-influenced zone. GWL, ranked second, acts as a background filter; low GWL values (blue points, down to -250) strongly reduce predicted risk, explaining its high global importance despite low local influence in LIME. GWL change, ranked third, is the most volatile active trigger, with high values (purple/red points, up to +350) providing the final “push” that drives high-probability subsidence predictions. Lithology (rank 4) contributes positively (~+200) where certain rock types are prone to subsidence, while proximity to faults (rank 6) can exert the strongest localized negative impact (~ -400), acting as structural weak points that dominate the model’s logic when present. Distance from rivers stretches to -300 for high values, indicating that being far from a river lowers risk. Together, these features illustrate how spatial, hydrogeological, and geological factors interact to control subsidence risk in the study area.

The key take away from study using XAI are the following:

- **Mining and Groundwater are key drivers:** The three most crucial drivers of risk are Distance from Mines, followed by Groundwater Level (GWL), and GWL Change, confirming that human activity and geohydrological dynamics are the drivers as stated in all XAI methods.
- **Structural Control Matters:** Global contribution from LIME shows the average directional influence of

features across all predictions, revealing that Lithology provides the strongest average negative protective push, countering the positive risk influence of Mines and Faults. The model has learned that the dominant or average litholog**y** in our study area is inherently resilient, consistently directing the prediction away from the high-risk outcome, even when other dangerous factors like proximity to a mine are present.

- **Model is Sparse:** The LightGBM model is highly selective, with most features having no impact on most locations as indicated by the SHAP points near 0, only activated to make a high-risk prediction when a feature's value is extreme.

Thus, the collective use of XAI methods indicate that PFI is needed to set the global policy priority, but it doesn't show how a feature works. Whereas, LIME is needed to identify systemic protective factors (like Lithology's average negative push), which PFI misses. Finally, SHAP is essential to locate the critical thresholds, the specific point where a feature's value moves from no impact state (SHAP ≈ 0) to high impact state (SHAP $\neq 0$), which neither PFI nor LIME can provide.

3.3 Susceptibility Classification and Validation

The final susceptibility map is masked based on the original EGMS spatial coverage to ensure that the results are presented only within areas supported by actual observations. Although interpolated EGMS data were used during the analysis to provide spatial continuity and avoid gaps, interpolation introduces uncertainty in regions without direct measurements. Therefore, the final map is restricted to the extent of the original EGMS data shown in Figure 12, ensuring that the reported susceptibility patterns are grounded in observed data and remain reliable for interpretation.

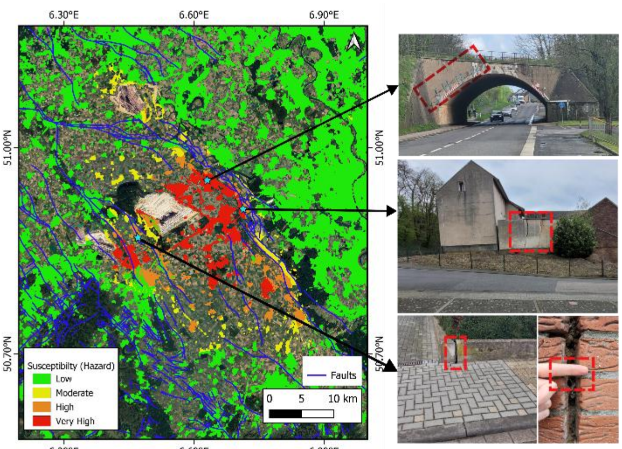

Figure 12. Final Suscpetibility map (left) with the faults(in blue) classified by LightGBM model showcasing the areas undergoing damages due to ongoing subsidence validated during our fieldwork.

The resulting susceptibility map in Figure 12 shows that high and very high risk zones are predominantly concentrated around mining areas. The right panel of Figure 12 highlights key observations: first, cracks along the overbridge fall within a very high susceptibility zone, representing a publicly accessible and hazardous area; second, severe wall damage occurs in the transition zone between very high and high susceptibility; and third, minor masonry defects are observed in transition areas of moderate to low susceptibility. This understanding enables stakeholders to interpret susceptibility patterns with greater confidence. Consequently, the findings support data-driven planning and targeted mitigation strategies. The integrated ML–XAI framework thus facilitates informed decision-making for sustainable regional management.

This understanding enables stakeholders to interpret susceptibility patterns with greater confidence. Consequently, the findings support data-driven planning and targeted mitigation strategies. The integrated ML–XAI framework thus facilitates informed decision-making for sustainable regional management.

4. Conclusion

This study demonstrates that subsidence susceptibility is strongly controlled by proximity to mining activities and groundwater dynamics, with high and very high risk zones predominantly concentrated around mining areas and validated by field observations. The integration of XAI techniques provides deeper insight into model behavior, confirming that Distance from Mines, Groundwater Level are the primary drivers, while lithology acts as a consistent protective factor and faults contribute to localized structural weakness. The LightGBM model exhibits selective behavior, responding primarily to extreme feature values, which enhances its reliability in identifying high-risk zones. Furthermore, the combined use of PFI, LIME, and SHAP enables a comprehensive interpretation by capturing global importance, average feature influence, and critical thresholds, respectively. Overall, the proposed ML–XAI framework not only improves prediction accuracy but also enhances transparency, supporting confident interpretation and enabling data-driven decision-making for effective risk mitigation and sustainable regional planning.

Acknowledgements

The authors would like to thank the Copernicus Data Space Ecosystem for providing Sentinel-2 data used in this study. We are grateful to Copernicus Land Monitoring Services for processing the EGMS data used as reference data in our study. We also acknowledge Erftverband for supplying groundwater data essential for the analysis. This research was partially supported by SARKI4Tagebaufolgen project financed via Bundesministerium für Wirtschaft und Energie (BMWE) in Germany.

References

Adadi, A., Berrada, M. (2018). Peeking Inside the Black-Box: A Survey on Explainable Artificial Intelligence (XAI). *IEEE Access*, *6*, 52138–52160. doi.org/10.1109/ACCESS.2018.2870052

Al-Masnay, Y. A., Al-Areeq, N. M., Ullah, K., Al-Aizari, A. R., Rahman, M., Wang, C., Zhang, J., Liu, X. (2022). Estimate earth fissure hazard based on machine learning in the Qa’ Jahran Basin, Yemen. *Scientific Reports*, *12*(1), 21936. doi.org/10.1038/s41598-022-26526-y

Bai, Z., Zhao, F., Wang, J., Li, J., Wang, Y., Li, Y., Lin, Y., Shen, W. (2025). Revealing long-term displacement and evolution of open-pit coal mines using sbas-insar and ds-insar. *Remote Sensing*, *17*(11), 1821. doi.org/10.3390/rs17111821

BGR (2016). (n.d.). [Dataset; Vector shapefile]. Geoportal der Bundesanstalt für Geowissenschaften und Rohstoffe. Retrieved https://geoportal.bgr.de/mapapps/resources/apps/geoportal/index.html?lang=de#/geoviewer?metadataId=8C6A2CA8-B4B9-48F7-8105-60D0AB4FF911

Breiman, L. (2001). Random forests. *Machine Learning*, *45*(1), 5–32. doi.org/10.1023/A:1010933404324

Crosetto, M., Cuevas-González, M., Mróz, M., Moldestad, D. A., Raspini, F., Casagli, N., Bateson, L., Novellino, A., Motagh, M., Guerrieri, L., Comerci, V. (2026). European Ground Motion Service: A decade of Sentinel-1 observations. *Remote Sensing of Environment*, *339*, 115389. doi.org/10.1016/j.rse.2026.115389

Firozjaei, M. K., Sedighi, A., Firozjaei, H. K., Kiavarz, M., Homaee, M., Arsanjani, J. J., Makki, M., Naimi, B., Alavipanah, S. K. (2021). A historical and future impact assessment of mining activities on surface biophysical characteristics change: A remote sensing-based approach. *Ecological Indicators*, *122*, 107264. doi.org/10.1016/j.ecolind.2020.107264

Ke, G., Meng, Q., Finely, T., Wang, T., Chen, W., Ma, W., Ye, Q., Liu, T. Y. (2017). *LightGBM: A highly efficient gradient boosting decision tree*. In Advances in Neural Information Processing Systems.

Lian, H., Yi, H., Yang, Y., Wu, B., Wang, R. (2021). Impact of coal mining on the moisture movement in a vadose zone in open-pit mine areas. *Sustainability*, *13*(8), 4125. doi.org/10.3390/su13084125

Liu, Y., Yang, T., Wang, H., Zhang, P., Dong, X., Zhao, Y., Liu, Y. (2024). Risk assessment of disaster chain in multi-seam mining beneath gully topography. *International Journal of Disaster Risk Reduction*, *111*, 104750. doi.org/10.1016/j.ijdrr.2024.104750

Lundberg, S., & Lee, S.-I. (2017). *A Unified Approach to Interpreting Model Predictions* (Version 2). arXiv. doi.org/10.48550/ARXIV.1705.07874

Mirmazloumi, S. M., Wassie, Y., Nava, L., Cuevas-González, M., Crosetto, M., Monserrat, O. (2023). InSAR time series and LSTM model to support early warning detection tools of ground instabilities: Mining site case studies. *Bulletin of Engineering Geology and the Environment*, *82*(10), 374. doi.org/10.1007/s10064-023-03388-w

Qiu, P., Liu, F., Zhang, J. (2023). Land subsidence prediction model based on the long short-term memory neural network optimized using the sparrow search algorithm. *Applied Sciences*, *13*(20), 11156. doi.org/10.3390/app132011156

Rahmati, O., Golkarian, A., Biggs, T., Keesstra, S., Mohammadi, F., Daliakopoulos, I. N. (2019). Land subsidence hazard modeling: Machine learning to identify predictors and the role of human activities. *Journal of Environmental Management*, *236*, 466–480. doi.org/10.1016/j.jenvman.2019.02.020

Ribeiro, M. T., Singh, S., Guestrin, C. (2016). Why Should I Trust You?: Explaining the Predictions of Any Classifier. *Proceedings of the 22nd ACM SIGKDD International Conference on Knowledge Discovery and Data Mining*, 1135–1144. doi.org/10.1145/2939672.2939778

Ritushree, D., Baes, M., Motagh, M. (2026). Hydrological and tectonic linkage to subsidence risk in the Rhineland coalfields, Germany: Integrating machine learning with remote sensing and geospatial data. *Engineering Geology*, *369*, 108751. doi.org/10.1016/j.enggeo.2026.108751

Tang, W., Motagh, M., Zhan, W. (2020). Monitoring active open-pit mine stability in the Rhenish coalfields of Germany using a coherence-based SBAS method. *International Journal of Applied Earth Observation and Geoinformation*, *93*, 102217. oi.org/10.1016/j.jag.2020.102217

The Council for the Environment and Infrastructure. (2020). Stop Land Subsidence in Peat Meadow Areas [Advisory Report]. https://www.rli.nl/sites/default/files/advisery_report_stop_land_subsidence_in_peat_meadow_areas.pdf

Wolersdorfer, C., Thiem, G. (1999). Ground Water Withdrawal and Land Subsidence in Northeastern Saxony (Germany). *Mine Water and the Environment*, *18*, 81–92.

Zhou, C., Cao, Y., Gan, L., Wang, Y., Motagh, M., Roessner, S., Hu, X., Yin, K. (2024). A novel framework for landslide displacement prediction using MT-InSAR and machine learning techniques. *Engineering Geology*, *334*, 107497. doi.org/10.1016/j.enggeo.2024.107497